age, ≥50 and KPS, ≥70; and surgical resection with good neurologic function.) were 17.9 and 11.1 months, respectively (5). Later, Filippini *et al.* (8) reported that surgery in patients with a good performance status improved survival irrespective of the patient's age. They mention that chemoradiotherapy improved survival regardless of age and performance status. More recently, use of radiotherapy plus temozolomide was shown to increase the median survival in a phase III randomized trial compared to use of external beam radiotherapy alone (9–11). Furthermore, early-stage clinical trials demonstrated that radiotherapy plus other types of molecule-targeted agents were tolerable, but their advantages have not yet been confirmed (12, 13).

As for radiotherapy alone, Tanaka *et al.* (14) reported that high-dose conformal radiotherapy of 80 to 90 Gy in 2-Gy daily fractions for malignant glioma had the potential to improve survival. Fitzek *et al.* (15) reported that conformal protons and photons in an accelerated fractionation of 90 GyE would improve local control and patient survival for GBM compared to the above-mentioned RTOG RPA data. Moreover, Mizoe *et al.* (16) reported the effectiveness of combined x-ray radiotherapy, carbon ion radiotherapy, and chemotherapy. However, there has been no high-level evidence that high-dose radiotherapy improves survival (17, 18). With these findings in mind and referring to the study reported by Fistzek *et al.* (15), we looked into the efficacy and safety of hyperfractionated concomitant boost proton radiotherapy for patients with supratentorial GBM.

METHODS AND MATERIALS

Patients

Between September 2001 and April 2008, 21 patients with GBM were prospectively enrolled in a phase I/II protocol for treatment with hyperfractionated concomitant boost proton radiotherapy. The eligibility criteria were as follows: (1) patients were newly diagnosed with supratentorial GBM; (2) patients were between 20 and 80 years old; (3) they had visibly enhanced residual tumor on magnetic resonance imaging (MRI) taken within 72 hours after surgery; (4) the diameter of the enhanced area before radiotherapy was ≤40 cm; (5) patients' KPS was ≥60%; and (6) the enhanced area did not extend to the brain stem, hypothalamus, or thalamus. Patients' diagnoses were histologically confirmed by two pathologists at the University Hospital of Tsukuba. One patient was excluded from this analysis because the diameter of the target volume was >4 cm after encompassing the entire surgical cavity. The enrollment status of this patient to this protocol was determined based on the patient's wishes and consent. As a result, this analysis was conducted on 20 cases which met the above criteria.

The group of 20 patients included 11 men and 9 women, with a median age of 57 years (range, 31–76 years). The distribution of KPS was as follows: 60 (n = 1 patient), 70 (n = 5 patients), 80 (n = 8 patients), 90 (n = 5 patients), and 100 (n = 1 patient). Seven patients underwent partial resection, and 13 patients underwent subtotal resection; there were no cases with gross total resection in this series. In the RTOG RPA classification, there were 3 cases in class III and 17 cases in class IV. The median MIB-1 (anti-Ki67 antibody) labeling index was 26.2% (range, 3.8%–55.0 %). Table 1 shows the characteristics of the 20 patients.

Table 1. Patient characteristics

Characteristics	No. of patients	Median
Age	range, 31-76 years	57
Gender		
Male	11	
Female	9	
Karnofsky performance status		
60	1	
70	5	
80	8	
90	5	
100	1	
Extent of surgery		
Partial resection	7	
Subtotal resection	13	
RPA class		
III	3	
IV	17	
MIB-1 labeling index (%)	3.8–55.0 (range)	26.2

Treatment methods

All patients received hyperfractionated concomitant boost proton radiotherapy after surgery. Treatment planning for proton beam therapy involved computed tomography (CT) images at 3-mm intervals at the treatment position. Proton beams of 250 MeV were generated by a booster synchrotron at the Proton Medical Research Center (PMRC), University of Tsukuba. The treatment planning system provided dose distributions and settings for the collimator configuration, bolus, and range shifter thickness. The relative biological effectiveness of the proton beam therapy was assumed to be 1.1 in this study (19). The clinical target volume 1 (CTV1) included the entire surgical bed or cavity in addition to any area of contrast enhancement on MRI. CTV2 was defined as the area of contrast enhancement plus a 10-mm margin. CTV3 was defined as the surrounding edema, determined by imaging studies (MRI T_2-weighted or fluid-attenuated inversion recovery), which includes CTV1/2. Conventional x-ray radiotherapy with 6 or 10 MV (50.4 Gy in 28 fractions) was delivered to CTV3 in the morning. In the first half of the protocol, additional concomitant boost proton radiotherapy (23.1 GyE in 14 fractions) was delivered to CTV2 more than 6 hours after x-ray radiotherapy. Then, in the latter half, proton radiotherapy (23.1 GyE in 14 fractions) was delivered to CTV1 instead of CTV2. The planning target volume (PTV) was defined as the clinical target volume plus 5 mm for setup error. As a result, the total dose for PTV1 was 96.6 GyE in 56 fractions, 73.5 GyE in 42 fractions for PTV2, and 50.4 Gy in 28 fractions for PTV. Nimustine hydrochloride (ACNU) was administered intravenously at a dose of 80 mg/m^2 for 1 day in the first and fourth weeks of external beam radiation therapy (Fig 1).

Follow-up procedures and evaluation criteria

During treatment, acute treatment-related toxicities were assessed weekly in all patients. After completion of the protocol, the patients were evaluated by physical examination, MRI, and blood tests every 2 months for the first year, at every 3 months for the second year, and at every 6 months thereafter if no neurological deterioration was observed. The Kaplan-Meier method was used to calculate local control and survival rates. Acute- and late-treatment-related toxicities were assessed using National Cancer Institute Common Criteria, version 3.0, and RTOG/EORTC late radiation morbidity scoring scheme (20).

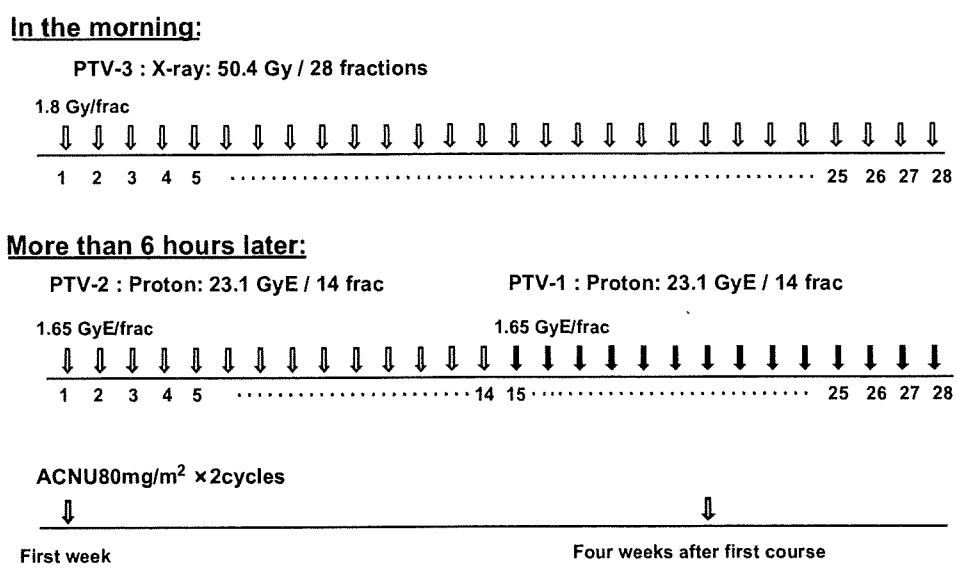

Fig. 1. A schematic diagram of the treatment protocol for GBM. ACNU was given intravenously at a dose of 80 mg/m^2 during the first and fourth weeks of external beam radiation therapy.

Considering the statements about posttreatment imaging analyses by Fitzek *et al* (15), we adopted the term "MRI change" instead of "progression" here, which designates an awareness or enlargement of an enhancing region on cross-sectional MRI after the protocol was completed. When two physicians, including one neuroradiologist, diagnosed a new contrast enhancement or an enlargement of an existing contrast enhancement on three-dimensional MRI, we considered that point an occurrence of MRI change. As it is frequently impossible to differentiate tumor progression from treatment effects such as pseudo-progression or radiation necrosis by MRI, especially soon after treatments, we did not use the conventional term "progression" at the premature stage. In-field MRI change was defined as this phenomenon observed mainly in the region inside CTV1 where 96.6 GyE was delivered. Border MRI change was defined as the phenomenon observed mainly in the regions of CTV2 or CTV3 where between 50.4 GyE and 96.6 GyE was delivered, and extra-field MRI change was defined as the phenomenon observed mainly in the region outside CTV3.

Ethics

The Ethical Committee and the Steering Committee of Proton Medical Research Center, University of Tsukuba, approved this clinical study in August 2001, and written informed consent was obtained from every patient prior to conducting this protocol study.

RESULTS

All patients received this protocol within 3 months postoperatively. The period between surgery and initiation of the protocol was 15 to 87 days (median, 27 days). All of the patients completed the protocol within 38 to 50 days (median, 43 days). Sixteen of 20 patients completed two cycles of ACNU, and the remaining 4 patients received one cycle of ACNU. There was no suspension of treatment except for one case (Table 3 patient 15) whose treatment had a 1-day pause due to cholecystitis which was treated by laparoscopic surgery.

Toxicity

As for acute toxicity, 4 cases were treated with corticosteroids during the protocol. In case 4, dexamethazone was administered for 5 days (from 4 mg/day to 0.5 mg/day), followed by oral administration of prednisolone for 7 days (from 20 mg/day to 5 mg/day) for headache and nausea due to an increase in the enhanced region and surrounding brain edema. In case 10, dexamethazone (4 mg/day) was administered continuously to control symptomatic edema after surgery, and the patient's dose was gradually decreased to zero during the early phase of the protocol. In cases 3 and 13, oral administration of prednisolone was started at 20 mg/day at 18 GyE and 30 GyE, respectively, in order to relieve symptoms of radiation sickness, which disappeared eventually after 10 to 14 days of steroid treatment. The fourth case (17) was treated with 250 mg of methyl prednisolone for skin eruption of unknown origin. There was grade 1 radiation dermatitis in cases 19 and 20, and grade 2 in 18 cases. One patient, a 55-year-old male who was excluded from this analysis due to the excessive size of CTV1, demonstrated a local skin infection for which an Ommaya reservoir was implanted. A skin graft was placed after the Ommaya reservoir was removed and debridement was performed. Ten patients had grade 3 or 4 leucopenia, 4 patients had grade 3 anemia, and 5 patients had grade 3 or 4 thrombocytopenia; considering the timing of the occurrence, the acute hematologic toxicities were probably caused by the administration of ACNU (Table 2). As a result, 3 patients needed blood transfusion and granulocyte colony-stimulating factor, and 5 patients needed granulocyte colony-stimulating factor.

As for late toxicity, it was difficult to clearly distinguish radiation necrosis from tumor recurrence in many cases, with MRI changes. Both toxicities were present in the pathology in 6 cases who underwent surgical removal due to symptomatic MRI changes after this protocol. Case 5 demonstrated the appearance of an enhanced region at the border of

Table 2. Therapy-related acute and late toxicity

Toxicity	Grade 0	1	2	3	4
Alopecia	0	0	20	—	—
Radiation dermatitis	0	2	18	0	0*
Rash	19	0	1*	0	0
Headache (including radiation sickness)	15	2	3*	0	0
Leucopenia	3	3	4	6	4
Anemia	3	10	3	4	0
Thrombocytopenia	4	6	5	3	2
Leukoencephalopathy associated radiological findings[†]	0	0	0	2[‡]	0

* Treated with steroids.

† Since pathological findings of 6 cases with reoperation demonstrated various degrees of mixture or necrosis and degenerated or viable tumor cells, these cases are not included here.

‡ A case of leukoencephalopathy (patient 11) and a case of radiation necrosis (patient 5).

the field 30 months after completion of treatment. Thereafter, this lesion rapidly increased in size with a large cyst formation, which strongly indicates radiation necrosis, although no pathological proof was available. Case 11 demonstrated no such changes on MRI after treatment. However, approximately 18 months after the end of the protocol, levels of consciousness and daily activity decreased gradually. MR images taken at this point demonstrated cortical atrophy with diffuse white matter change on T_2-weighted MRI, which strongly indicates leukoencephalopathy. The CTV1 of this patient was 152.2 cc, which is the second largest in this series. This patient became bedridden without evidence of tumor recurrence and died of respiratory insufficiency, most probably due to pulmonary embolism.

Response

The 1- and 2-year MRI change-free survival rates of the 20 patients were 45.0% and 15.5%, respectively. The median time to occurrence of MRI change was 11.2 months (range, 3.4–24.6 months; 95% confidence interval [CI], 5.3–17.2 months). Fourteen of 20 patients had MRI changes; 4 patients had MRI changes mainly in the regions inside CTV1 (where 96.6 GyE was irradiated); 5 patients had MRI changes mainly in the region of CTV2 or CTV3 (where >50.4 GyE was irradiated, but <96.6 GyE was irradiated); and 5 patients had MRI changes in the regions mainly outside the irradiated field. Six of 14 patients who had MRI changes underwent reoperation 14 to 210 days after this protocol was completed. Among 4 patients with an in-field MRI change, 3 patients underwent reoperation, followed by administration of temozolomide or a combination therapy with procarvasin, ACNU, vincristine (PAV), and interferon-gamma. In addition, salvage immunotherapy was performed for 2 patients. As for 5 patients with border MRI change, 2 cases underwent reoperations followed by salvage immunotherapy with or without PAV as indicated. Two cases received chemotherapy with temozolomide or a combination of cisplatin and etoposide. The remaining case (patient 5) had no additional treatment according to the patient's wishes. Among 5 patients who demonstrated extra-field MRI change, 3 patients received additional proton beam or stereotactic x-ray radiotherapy with or without the combination of reoperation, chemotherapy,

Table 3. Patient characteristics

Patient	Age (y)	Sex	KPS (%)	Tumor location	RPA class	Surgery	CTV1 (cc)	MRI change-free survival (months)	Pattern of MRI change	Overall survival (months)	Follow-up and status
1	71	M	80	Lt Temporal	IV	Subtotal	12.6	12.6	Extra-field	18.7	Died of tumor
2	55	M	80	Rt Parietal	IV	Partial	57.6	11.2	In-field	32.1	Died of tumor
3	54	M	70	Lt Parietal	IV	Partial	42.3	7.4	In-field	21.6	Died of tumor
4	31	M	80	Lt Frontal	IV	Partial	55.2	3.4	Border	7.2	Died of tumor
5	61	M	80	Rt Temporal	IV	Partial	14.7	16.7	Border	47.9	Alive
6	45	M	80	Lt Temporal	IV	Subtotal	42.9	6.5	Border	10.7	Died of tumor
7	63	F	70	Lt Frontal	IV	Subtotal	88.8	4.2	Border	25.6	Died of tumor
8	46	F	60	Rt Temporal	IV	Subtotal	56.6	5.1	Extra-field	42.8	Died of tumor
9	62	F	90	Lt Frontal	IV	Subtotal	22.8	8.2	Extra-field	10.5	Died of tumor
10	56	M	80	Rt. Occipital	IV	Partial	108.0	6.1	Extra-field	11.7	Died of tumor
11	76	M	70	Rt Temporal	IV	Subtotal	152.2	20.4	None	20.4	Died of RI
12	76	F	70	Lt Temporal	IV	Subtotal	167.0	12.2	Extra-field	21.5	Died of tumor
13	49	F	90	Lt Parietal	III	Subtotal	46.2	7.1	In-field	25.7	Alive
14	65	F	70	Rt Frontal	IV	Subtotal	38.4	24.6	None	24.6	Alive
15	59	M	80	Rt Temporal	IV	Partial	51.2	6.4	None	6.4	Died of sepsis
16	31	M	80	Rt Frontal	IV	Partial	26.5	14.1	In-field	35.0	Alive
17	46	F	90	Rt Frontal	III	Subtotal	14.6	12.2	None	12.8	Alive
18	61	M	90	Rt Frontal	IV	Subtotal	76.3	3.9	Border	3.9	Alive
19	42	F	100	Lt Temporal	III	Subtotal	13.4	5.2	None	5.2	Alive
20	58	F	90	Rt Temporal	IV	Subtotal	3.0	10.0	None	10.0	Alive

Abbreviations: Rt = right; Lt = left; RI = respiratory insufficiency.

or immunotherapy as shown in Fig. 2. One patient (case 1) refused any additional therapy. The pathology of 6 patients who underwent reoperation demonstrated mainly a mixture of necrosis, interstitial edema, and degenerated residual GBM cells.

Survival

The overall survival rates after 1 and 2 years were 71.1% and 45.3%, respectively. The median survival periods were 21.6 months (range, 3.9–47.9 months; 95% CI, 15.5–27.7 months). Figure 3 shows the overall survival and MRI change-free survival rates. At the time of analysis, 8 patients were alive and 12 patients were dead; the median follow-up period for survivors was 24.6 months. Ten of 12 patients died of tumor recurrence, and the other 2 patients died of diseases that were not related to tumor recurrence. As mentioned in *Toxicity* (above), one patient (case 11) died of respiratory insufficiency and a disturbance of consciousness 20.4 months after the initial surgery, although there was no evidence of tumor recurrence on the last MRI. The patient's KPS before radiotherapy was 70 %. The other patient (case 15) died of sepsis following cholelithiasis with cholecystitis and panperitonitis 6.4 months after the initial surgery. This patient had moderate diabetes, and the KPS before radiotherapy was 80 %. Table 3 shows the list of outcomes of the patients in this protocol.

It was difficult to distinguish treatment effect from tumor progression at the occurrence of MRI change. Although the eventual diagnosis of "recurrence" can be made based on progression in clinical symptoms and follow-up imaging studies, the precise point of recurrence is frequently difficult to determine because treatment effect and tumor progression might be continuous or mixed. Most patients in this study underwent nuclear medical studies using thallium-201 single-photon emission tomography at some point during the course of follow-up. However, they demonstrated moderately "hot" uptake in the area corresponding to enhancement on MRI in every case, indicating that the diagnostic role was not conclusive.

DISCUSSION

Radiotherapy is the standard treatment for high-grade gliomas after surgical resection because extensive tumor cells remain in the adjacent normal brain tissue. At present, the standard radiotherapy schedule used for patients with GBM is 60 Gy in 30 fractions (9–13). Owing to recent technological advancements in x-ray radiotherapy (*e.g.*, three-dimensional conformal radiation therapy and stereotactic radiosurgery/intensity-modulated radiation therapy), better dose localization to the tumor volume can be achieved. Several prospective studies using these techniques have shown that dose escalation with or without hypofractionation is feasible and that survival is not inferior to standard schedules (15–18, 21–23).

Fitzek *et al.* (15) reported that accelerated fractionated proton/photon irradiation to 90 GyE for GBM achieved better survival, with a median survival period of 20 months. More recently, Mizoe *et al.* (16) reported the results of a phase I/II trial involving combination therapy of carbon ion and x-ray for GBM, with doses ranging from 66.8 to 74.8 GyE,

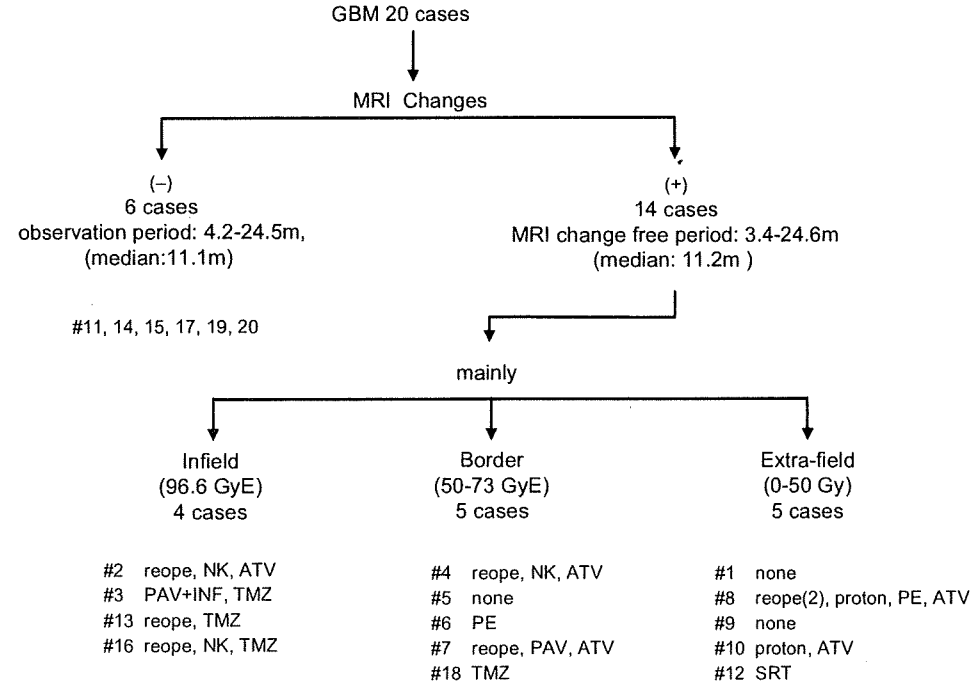

Fig. 2. Patterns of MRI changes and treatment methods after the occurrence of MRI changes. m = month(s); # = number of patients in Table 3; reope = reoperation; PAV = procarvasin plus ACNU plus vincristine; INF = interferon-gamma; TMZ = temozolomide; PE = cisplatin plus etoposide; SRT = stereotactic radiotherapy; NK = natural killer cell therapy; ATV = autologous tumor vaccine.

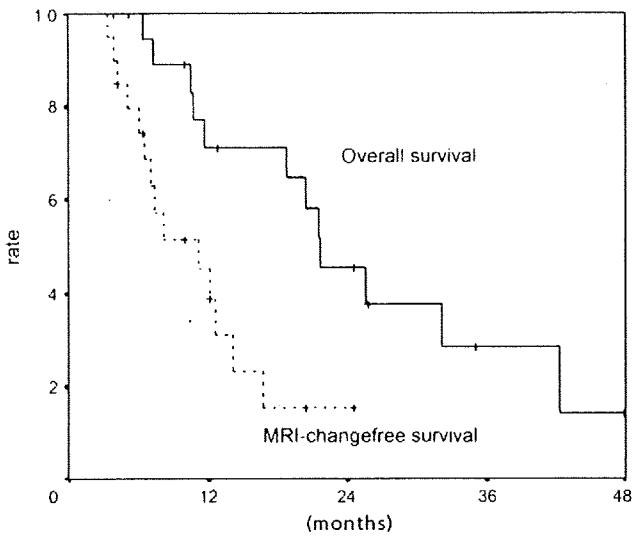

Fig. 3. Kaplan-Meier estimates of overall survival rate and progression-free survival rate for all 20 patients.

yielding a median survival period of 17 months. Compared to the standard schedule x-ray radiotherapy, with a median survival of <15 months (9, 10) or recent IMRT treatments with or without boost and hypofractionation (22, 23), those particle studies, including our present study, may indicate that dose escalation with particle radiotherapy has a potential to improve survival; nevertheless, prominent improvement has not yet been achieved.

It has been reported that age, extent of tumor resection, performance status, tumor size, and tumor location are prognostic factors for survival of patients with GBM (7, 24–26). In addition, Mirimanoff *et al.* (27) determined whether RPA retains its overall prognostic value and what the benefit of concurrent temozolomide is in each RPA class. The overall survival was statistically different among RPA classes III and IV, with median survival times of 17 and 15 months, respectively. Although there are selection biases, *e.g.*, tumors treated were <4 cm in diameter and did not involve risky regions, our data showed better survival, with a median survival period of 21.6 months, than that for the patients of RPA class III, despite the fact that 17 of 20 patients were classified as RPA class IV (Tables 1 and 3).

There has been no prospective large-scale phase I dose escalation study, until the recent report of Tsien *et al.* (28), who reported the results of a multiinstitutional clinical study in which the dose was escalated from 66 to 84 Gy, using a uniform three-dimensional conformal x-ray radiotherapy protocol (33). That study's results indicated that doses up to 84 Gy were well tolerated; however, a definitive survival advantage was not demonstrated, except for 22 cases in which PTV2 (gross tumor volume plus 0.3 cm) were treated with <75 ml and 84 Gy. The median survival of that cohort was 19.4 months, which might be due to not only smaller tumor size with a high dose delivery but also to a high rate of gross total resection (64%).

The most common failure pattern has been reported as local failure in GBM (17, 18). In our study, the occurrence of MRI changes was almost equal in the in-field, border, and extra-field areas (Fig. 3). Fitzek *et al.* (15) reported that all patients developed new areas of gadolinium enhancement during the follow-up period and that enhancements first occurred within the high-dose target volume. However, only 1 of 23 patients had recurrent tumor in the area that received 90 GyE consequently, and the most common failure was in the area that received 60 to 70 GyE or less. Although we agree that tumor control in the border area is a significant subject, prevention of border failure by radiotherapy alone may not be achievable at this time because of uncertainty as to the feasibility of delivering 90 GyE or more to larger PTV, even by using particle radiotherapy.

Cutoff values of tumor size were mentioned in some clinical trials with conformal radiotherapy before this protocol was started. Shaw *et al.* selected solitary recurrent tumors of ≤40 mm in maximum diameter for single- fraction radiosurgery for previously irradiated (60 Gy) recurrent primary brain tumors (29). They reported that the maximum tolerance dose of single-fraction radiosurgery depends on the size of the tumor, and it was 15 Gy for tumors of 31 to 40 mm. Also, Cho *et al.* treated recurrent high-grade gliomas with single- or fractionated stereotactic radiotherapy (30). Volumes of tumors treated in that study were 1 to 54 ml in SRS and 4 to 115 ml in stereotactic radiotherapy. Values of 54 ml and 115 ml are approximately equal to 4.6-cm- and 6.0-cm-diameter spheres, respectively. Finally, Fitzek *et al.* (15) selected patients whose tumor size was less than 60 ml (approximately equal to the largest postoperative diameter of 5 cm). Their clinical target volume (V1) for 90 GyE was the signal-intense rim of the tumor or the remaining cavity plus any residual enhancement on MRI. However, there are no comments on the safety margin in planning V1. Based on these parameters, we selected 4 cm as a cutoff diameter in this study because we added a 5-mm safety margin (1-cm margin in diameter) for clinical target volume, and our dose prescription to the core CTV was 6.6 GyE higher than theirs.

One patient who was treated with this protocol but excluded from analysis had a grade 4 skin injury, and this patient's overall survival period was 16.3 months, indicating that eventual benefit was not remarkable in this case. The CTV1 of this patient was 344.3 cc after encompassing the entire surgical cavity. Combined with the occurrence of leukoencephalopathy in case 11, whose CTV1 was 152.2 cc, we consider that delivering a high dose to a large CTV1 has a high risk; in addition, it might be difficult with this protocol to cover tumor invasion volume by CTV2 or CTV3 if CTV1 is more than 200 cc. Other acute toxicities were within the controllable range, indicating that doses of up to 96.6 GyE are tolerable if the target size is within a range indicated in this study.

As for late toxicity in high-dose radiotherapy for glioblastoma, Tanaka *et al.* (14) reported that 2 of 13 patients who received 90 Gy demonstrated radiation necrosis, diagnosed by biopsy or proton emission tomography images. Also, Fitzek *et al.* (15) mention that 7 of 23 cases who underwent

90 GyE of proton/photon irradiation demonstrated only necrosis, and the remaining 16 patients are thought to have had a mixture of radiation necrosis and recurrent tumor. Tsien *et al.* (28) mention that 8 cases demonstrated grade 3 or 4 radiation necrosis among 209 patients enrolled in their study of dose escalation from 66 to 84 Gy; however, its occurrence was not dose and volume related. In addition, pathological materials taken at the second surgery in 10 cases in their series demonstrated both recurrent GBM, as well as changes consistent with radiotherapy effects. Therefore, MRI changes after radiation doses of 96.6 GyE in our series probably demonstrate a mixture of radiation necrosis and tumor with or without recurrence in the field along the course of observation. Recently, several reports have shown the concept of radiation-induced pseudo-progression (31-33). Pseudo-progression is defined as the increase in size of contrast-enhancing lesions, or new areas with contrast enhancement, immediately after radiotherapy, with subsequent improvement without any further treatment. In our study, compared to a median overall survival period of 21.6 months, a median time to occurrence of MRI change of 11.2 months seemed relatively short. This may indicate that the MRI change in our series included pseudo-progression as well as radiation necrosis. Although detailed histopathological analyses concerning these phenomena are expected, it is beyond the scope of this paper. The other possible reason for prolonged survival period from the occurrence of MRI change might be various combinations of additional or salvage therapy which included reoperation, proton or x-ray irradiation, chemotherapy, or tumor immunotherapy. Although the authors believe that each therapy, including experimental salvage immunotherapy, contributed to some extent to the prolonged survival period, there was no dramatic tumor volume reduction resulting from these additional therapies.

After the results of a randomized phase III trial were published by Stupp *et al.* (10), the use of temozolomide therapy for patients with newly diagnosed GBM was approved in many countries in 2005, and it was approved in 2006 in Japan. Although temozolomide is now accepted as the standard chemotherapy for GBM, postoperative radiotherapy concurrent with ACNU was considered the standard treatment for GBM in Japan in 2001 when this protocol was started (34). This is the reason why we used ACNU in this protocol. Therefore, further clinical trials may be desirable to pursue safety and efficacy of concurrent use of temozolomide with our proton radiotherapy regimen.

CONCLUSIONS

In conclusion, hyperfractionated concomitant boost proton radiotherapy of 96.6 GyE in 56 fractions for supratentorial GBM is tolerable if the target size is well considered. The median survival time was extended to 21.6 months, which is one of the most favorable results reported to date. Further studies are warranted to reveal the effectiveness of dose escalation by proton beams and to pursue the possibility of concurrent therapy with other modalities to control the tumor border region.

REFERENCES

1. Walker MD, Strike TA, Sheline GE. An analysis of dose-effect relationship in the radiotherapy of malignant gliomas. *Int J Radiat Oncol Biol Phys* 1979;5:1725–1731.
2. Walker MD, Green SB, Byar DP, *et al.* Randomized comparisons of radiotherapy and nitrosoureas for the treatment of malignant glioma after surgery. *N Engl J Med* 1980;303: 1323–1329.
3. Fine HA, Dear KB, Loeffler JS, *et al.* Meta-analysis of radiation therapy with and without adjuvant chemotherapy for malignant gliomas in adults. *Cancer* 1993;71:2585–2597.
4. Stewart LA. Chemotherapy in adult high-grade glioma: A systematic review and meta-analysis of individual patient data from 12 randomised trials. *Lancet* 2002;359:1011–1018.
5. Curran WJ Jr., Scott CB, Horton J, *et al.* Recursive partitioning analysis of prognostic factors in three Radiation Therapy Oncology Group malignant glioma trials. *J Natl Cancer Inst* 1993;85: 704–710.
6. Scott CB, Scarantino C, Urtasun R, *et al.* Validation and predictive power of Radiation Therapy Oncology Group (RTOG) recursive partitioning analysis classes for malignant glioma patients: A report using RTOG 90-06. *Int J Radiat Oncol Biol Phys* 1998;40:51–55.
7. Lamborn KR, Chang SM, Prados MD. Prognostic factors for survival of patients with glioblastoma: Recursive partitioning analysis. *Neuro Oncol* 2004;6:227–235.
8. Filippini G, Falcone C, Boiardi A, *et al.* Prognostic factors for survival in 676 consecutive patients with newly diagnosed primary glioblastoma. *Neuro Oncol* 2008;10:79–87.
9. Athanassiou H, Synodinou M, Maragoudakis E, *et al.* Randomized phase II study of temozolomide and radiotherapy compared with radiotherapy alone in newly diagnosed glioblastoma multiforme. *J Clin Oncol* 2005;23:2372–2377.
10. Stupp R, Mason WP, van den Bent MJ, *et al.* Radiotherapy plus concomitant and adjuvant temozolomide for glioblastoma. *N Engl J Med* 2005;352:987–996.
11. Stupp R, Dietrich PY, Ostermann Kraljevic S, *et al.* Promising survival for patients with newly diagnosed glioblastoma multiforme treated with concomitant radiation plus temozolomide followed by adjuvant temozolomide. *J Clin Oncol* 2002;20: 1375–1382.
12. Moyal EC, Laprie A, Delannes M, *et al.* Phase I trial of tipifarnib (R115777) concurrent with radiotherapy in patients with glioblastoma multiforme. *Int J Radiat Oncol Biol Phys* 2007; 68:1396–1401.
13. Krishnan S, Brown PD, Ballman KV, *et al.* Phase I trial of erlotinib with radiation therapy in patients with glioblastoma multiforme: Results of North Central Cancer Treatment Group protocol N0177. *Int J Radiat Oncol Biol Phys* 2006;65: 1192–1199.
14. Tanaka M, Ino Y, Nakagawa K, *et al.* High-dose conformal radiotherapy for supratentorial malignant glioma: A historical comparison. *Lancet* 2005;6:953–960.
15. Fitzek MM, Thornton AF, Rabinov JD, *et al.* Accelerated fractionated proton/photon irradiation to 90 cobalt Gray equivalent for glioblastoma multiforme: Results of a phase II prospective trial. *J Neurosurg* 1999;91:251–260.
16. Mizoe JE, Tsujii H, Hasegawa A, *et al.* Phase I/II clinical trial of carbon ion radiotherapy for malignant gliomas: Combined X-ray radiotherapy, chemotherapy, and carbon ion radiotherapy. *Int J Radiat Oncol Biol Phys* 2007;69:390–396.

17. Cardinale R, Won M, Choucair A, *et al.* A phase II trial of accelerated radiotherapy using weekly stereotactic conformal boost for supratentorial glioblastoma multiforme: RTOG 0023. *Int J Radiat Oncol Biol Phys* 2006;65:1422–1428.
18. Souhami L, Seiferheld W, Brachman D, *et al.* Randomized comparison of stereotactic radiosurgery followed by conventional radiotherapy with carmustine to conventional radiotherapy with carmustine for patients with glioblastoma multiforme: Report of Radiation Therapy Oncology Group 93-05 protocol. *Int J Radiat Oncol Biol Phys* 2004;60:853–860.
19. Gerweck LE, Kozin SV. Relative biological effectiveness of proton beams in clinical therapy. *Radiother Oncol* 1999;50: 135–142.
20. National Cancer Institute. National Cancer Institute common toxicity criteria. http://ctep.cancer.gov/reporting/ctc.html.
21. Sultanem K, Patrocinio H, Lambert C, *et al.* The use of hypofractionated intensity-modulated irradiation in the treatment of glioblastoma multiforme: preliminary results of a prospective trial. *Int J Radiat Oncol Biol Phys* 2004;58:247–252.
22. Floyd NS, Woo SY, Teh BS, *et al.* Hypofractionated intensity-modulated radiotherapy for primary glioblastoma multiforme. *Int J Radiat Oncol Biol Phys* 2004;58:721–726.
23. Fuller CD, Choi M, Forthuber B, Wang SJ, Rajagiriyil N, Salter BJ, Fuss M. Standard fractionation intensity modulated radiation therapy (IMRT) of primary and recurrent glioblastoma multiforme. *Radiat Oncol* 2007;2:26.
24. Donato V, Papaleo A, Castrichino A, *et al.* Prognostic implication of clinical and pathologic features in patients with glioblastoma multiforme treated with concomitant radiation plus temozolomide. *Tumori* 2007;93:248–256.
25. Slotman BJ, Kralendonk JH, van Alphen HA, *et al.* Hypofractionated radiation therapy in patients with glioblastoma multiforme: Results of treatment and impact of prognostic factors. *Int J Radiat Oncol Biol Phys* 1996;34:895–898.
26. Gorlia T, van den Bent MJ, Hegi ME, *et al.* Nomograms for predicting survival of patients with newly diagnosed glioblastoma: Prognostic factor analysis of EORTC and NCIC trial 26981-22981/CE.3. *Lancet* 2008;9:29–38.
27. Mirimanoff RO, Gorlia T, Mason W, *et al.* Radiotherapy and temozolomide for newly diagnosed glioblastoma: Recursive partitioning analysis of the EORTC 26981/22981-NCIC CE3 phase III randomized trial. *J Clin Oncol* 2006;24:2563–2569.
28. Tsien C, Moughan J, Michalski JM, *et al.* Phase I three-dimensional conformal radiation dose escalation study in newly diagnosed glioblastoma: Radiation therapy oncology group trial 98-03. *Int J Radiat Oncol Biol Phys.* 2009;73:699–708.
29. Shaw E, Scott C, Souhami L, *et al.* Single dose radiosurgical treatment of recurrent previously irradiated primary brain tumors and brain metastases: Final report of RTOG protocol 90-05. *Int J Radiat Oncol Biol Phys* 2000;47:291–298.
30. Cho KH, Hall WA, Gerbi BJ, *et al.* Single dose versus fractionated stereotactic radiotherapy for recurrent high-grade gliomas. *Int J Radiat Oncol Biol Phys* 1999;45:1133–1141.
31. Brandsma D, Stalpers L, Taal W, *et al.* Clinical features, mechanisms, and management of pseudoprogression in malignant gliomas. *Lancet* 2008;9:453–461.
32. Taal W, Brandsma D, de Bruin HG, *et al.* Incidence of early pseudo-progression in a cohort of malignant glioma patients treated with chemoirradiation with temozolomide. *Cancer* 2008;113:405–410.
33. Brandes AA, Franceschi E, Tosoni A, *et al.* MGMT promoter methylation status can predict the incidence and outcome of pseudoprogression after concomitant radiochemotherapy in newly diagnosed glioblastoma patients. *J Clin Oncol* 2008;26: 2192–2197.
34. Takakura K, Abe H, Tanaka R, *et al.* Effects of ACNU and radiotherapy on malignant glioma. *J Neurosurg* 1986;64: 53–57.

Acta Oncologica, 2009; 48: 314–318

informa
healthcare

LETTERS TO THE EDITOR

Contrast media-assisted visualization of brain metastases by kilovoltage cone-beam CT

HIROSHI IGAKI[1], KEIICHI NAKAGAWA[1], HIDEOMI YAMASHITA[1], ATSURO TERAHARA[1], AKIHIRO HAGA[1], KENSHIRO SHIRAISHI[1], NAKASHI SASANO[1], KENTARO YAMAMOTO[1], TSUYOSHI ONOE[1,2], KIYOSHI YODA[3] & KUNI OHTOMO[1]

[1]*Department of Radiology, University of Tokyo Hospital, Tokyo, Japan,* [2]*Department of Radiation Oncology, Cancer Institute Hospital, Tokyo, Japan and* [3]*Elekta, KK, Kobe, Japan.*

To the Editor

The latest linear accelerator equipped with a kilovoltage (kV) cone-beam CT (CBCT) unit is useful for registration at the time of treatment, and thus reduces the setup error [1–4]. But in the case of intracranial or abdominal tumors, the contours of the tumors are difficult to determine on the CT images without contrast media, since such tumors are located next to normal soft tissue whose Hounsfield unit is close to those of the tumors themselves.

Image registration by CBCT is performed based on the bony structures or soft tissue around the tumor. But this process does not necessarily guarantee that the position of the isocenter at treatment is identical with that at the time of planning CT, since bone or soft-tissue registration is based on a volume-matching process. It is difficult to know the exact tumor location for a low-contrast tumor even if on-board registration of the tumor is intended, since the tumor contour is not well visualized even on planning CT images without contrast media. We attempted to visualize metastatic brain

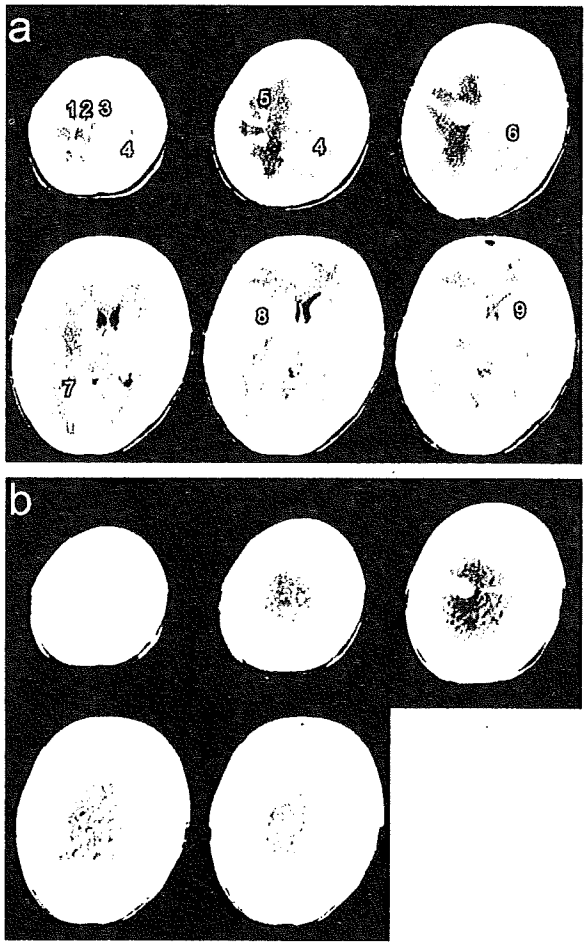

Figure 1 (*Continued*)

Figure 1. Brain tumor images acquired by planning CT (a) and kV CBCT (b) after each intravenous bolus administration of iodized contrast media. The treatment isocenter was set within the tumor indicated by the arrow. Tumors are indicated by the arrowhead. All tumors 6 mm or more in the greatest dimension in the planning CT (a) were also detectable in the CBCT (b). The numbers assigned in the tumor correspond to those in Table I.

Correspondence: Keiichi Nakagawa, Department of Radiology, University of Tokyo Hospital, 7-3-1 Hongo, Bunkyo-ku, Tokyo, 113-8655, Japan. Tel: +81 3 5800 8666. Fax: +81 3 5800 8786. E-mail: k-nak@fg7.so-net.ne.jp

(Received 6 June 2008; accepted 30 June 2008)

ISSN 0284-186X print/ISSN 1651-226X online
DOI: 10.1080/02841860802310983

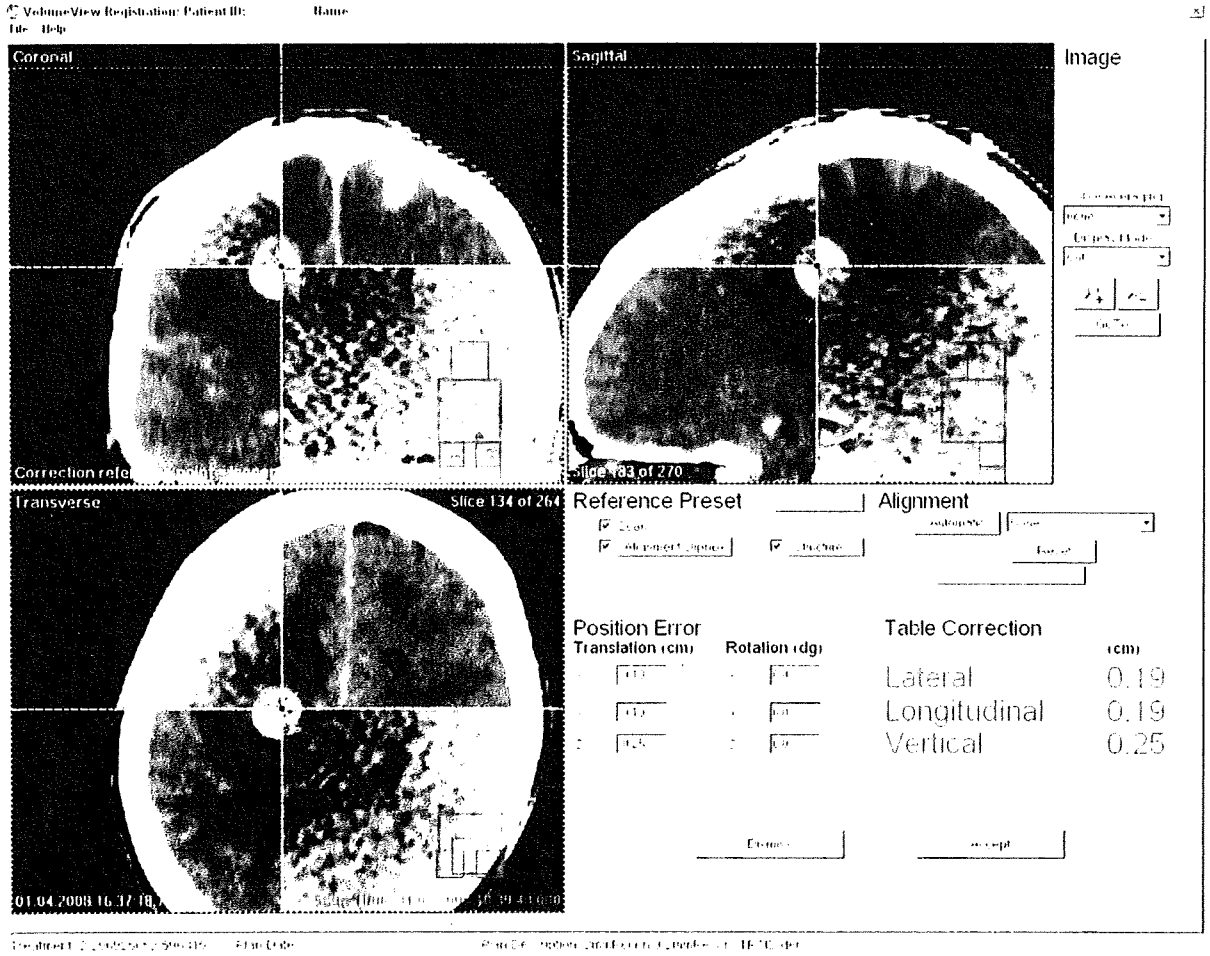

Figure 2. The desktop screen at the time of image registration. After bone registration, the location of the tumor at the isocenter was verified by eye and registered well.

tumors by contrast media administration in kV CBCT images.

A 41-year-old female developed multiple brain metastases from a follicular variant of papillary carcinoma of the thyroid. Radiotherapy planning was performed by Pinnacle[3] (Philips/ADAC, Milpitas, CA) based on CT images acquired by a large-bore CT (Aquilion/LB, Toshiba, Tokyo, Japan) after an intravenous bolus injection of 100 ml of iodized contrast media, Iopamiron 300 (Schering, Berlin,

Table I. Characteristics of the tumors observed in the planning CT.

Tumor No.[1]	Size (mm)[2]	Locus	Possible factors interfering with detectability in CBCT [8]
1	6×4	Rt. high frontal	Cupping artifacts Ring artifact
2	7×5	Rt. high frontal	Cupping artifacts Ring artifact
3	18×16	Lt. high frontal	Cupping artifacts Ring artifact
4	27×19	Lt. high frontal	Cupping artifacts Ring artifact
5	7×7	Rt. high frontal	Cupping artifacts
6	19×16	Rt. frontal	–
7	8×8	Rt. occipital	Cupping artifacts
8	7×7	Rt. frontal tip	Ring artifact
9	8×8	Lt. frontal tip	Ring artifact
10	4×4	Lt. frontal	Cupping artifacts Ring artifact

[1]The numbers of the tumors correnspond to those in Figure 1.
[2]Sizes were measured on 5-mm-thick images of the planning CT.
The greatest dimension and its orthogonal dimension in the axial slice was presented.

Germany). Elekta Synergy (Elekta, Crawley, England), equipped with kV CBCT unit, was used for registration and treatment. Immediately before the treatment, on-board CBCT images were taken four minutes after another intravenous bolus injection of 100 ml of Iopamiron 300. The initial estimation of the tumor registration was performed by built-in bone-matching software because it was very quick. Subsequently, the tumor position in the CBCT image and the isocenter imported from the treatment planning system were displayed for further manual adjustment by eye. Written informed consent on these procedures and treatment was obtained from the patient.

Figure 1a presents representative axial images of the planning CT of this patient. Figure 1b shows kV CBCT images of the corresponding slices taken immediately before the treatment. The isocenter was set within the tumor in the right frontal lobe indicated by the arrow in the Figure 1a. No further manual adjustment was performed after bone matching in this study. The tumor position was directly registered (Figure 2). Thus, it was shown that direct tumor registration was feasible by contrast media-assisted kV CBCT. The patient was treated with whole-brain irradiation.

All the tumors with diameters of 6 mm or more in the greatest dimension observed in the 5-mm-thickness planning CT image were also visible by CBCT (Table I). Ring artifacts of the concentric circle that centers on the treatment isocenter, possibly due to the skull, were seen in the CBCT images (Figure 1b). But these artifacts did not degrade the accuracy of visual verification insofar as the tumor was detectable. Other smaller metastases sized less than 6 mm in the planning CT were undetectable in the CBCT images.

This is the first report of direct tumor visualization and registration in the linear accelerator-mounted CBCT by contrast media administration. It had been reported that sufficient soft-tissue contrast could not be obtained in kV CBCT images by contrast media administration [5]. This is an obstacle for direct tumor registration. To overcome this difficulty, Guckenberger et al. used mobile in-room CT with contrast media just before the treatment [5,6]. The idea of their report is interesting, but the tumor image obtained by in-room CT does not warrant exact tumor position during the treatment. Through our procedure, we can know the exact position of the small tumor itself in an organ with soft-tissue density on-board even during the treatment by simultaneous dual exposure of kV x-ray for CBCT and megavoltage x-ray for treatment [4]. In addition, we determined the minimum size of brain tumors that can be visualized by kV CBCT in this study.

Metastatic brain tumors 6mm or more in the greatest dimension were visualized in the CBCT. This means that tumors 6 mm or more in the greatest dimension are candidates for direct tumor registration by contrast media-assisted kV CBCT. The possible reasons why smaller tumors could not be detected in the CBCT were low contrast of the image, low resolution of the image, the ring artifacts described above, and artifacts due to beam hardening. Most of them had been pointed out previously [7,8], and some problems have already overcome by improvement of the systems [7].

The tumors of the patient involved in this report were strongly and homogeneously enhanced by contrast media. Such characteristics of the tumor appeared suitable for this procedure of visualization. In our preliminary experience, soft-tissue contrast of cystic tumors or heterogeneously enhanced tumors was insufficient in the CBCT images. It is expected that the radiological characteristics of the tumor influence the minimum size of the tumor that can be visualized by CBCT. In the future, we should clarify such relationships by further studies incorporating more patients.

Conflict of Interest Statement

Dr. Nakagawa receives research funding from Elekta K.K. All other authors have no financial or personal relationship with other people or organizations that could inappropriately influence this work.

References

[1] Oldham M, Letourneau D, Watt L, Hugo G, Yan D, Lockman D, et al. Cone-beam-CT guided radiation therapy: A model for on-line application. Radiother Oncol 2005;75: 271–8.

[2] Boda-Heggemann J, Walter C, Rahn A, Wertz H, Loeb I, Lohr F, et al. Repositioning accuracy of two different mask systems-3D revisited: Comparison using true 3D/3D matching with cone-beam CT. Int J Radiat Oncol Biol Phys 2006; 66:1568–75.

[3] Thilmann C, Nill S, Tucking T, Hoss A, Hesse B, Dietrich L, et al. Correction of patient positioning errors based on in-line cone beam CTs: Clinical implementation and first experiences. Radiat Oncol 2006;1:16.

[4] Nakagawa K, Yamashita H, Shiraishi K, Igaki H, Terahara A, Nakamura N, et al. Verification of in-treatment tumor position using kilovoltage cone-beam computed tomography: A preliminary study. Int J Radiat Oncol Biol Phys 2007;69: 970–3.

[5] Guckenberger M, Baier K, Guenther I, Richter A, Wilbert J, Sauer O, et al. Reliability of the bony anatomy in image-guided stereotactic radiotherapy of brain metastases. Int J Radiat Oncol Biol Phys 2007;69:294–301.

[6] Guckenberger M, Sweeney RA, Wilbert J, Krieger T, Richter A, Baier K, et al. Image-guided radiotherapy for liver cancer using respiratory-correlated computed tomography and cone-

beam computed tomography. Int J Radiat Oncol Biol Phys 2008;71:297–304.
[7] Letourneau D, Wong JW, Oldham M, Gulam M, Watt L, Jaffray DA, et al. Cone-beam-CT guided radiation therapy: Technical implementation. Radiother Oncol 2005;75:279–86.
[8] Barrett JF, Keat N. Artifacts in CT: Recognition and avoidance. Radiographics 2004;24:1679–91.

J Neurosurg 111:520–526, 2009

Arcuate fasciculus tractography integrated into Gamma Knife surgery

Clinical article

KEISUKE MARUYAMA, M.D., PH.D.,[1] TOMOYUKI KOGA, M.D.,[1] KYOUSUKE KAMADA, M.D., PH.D.,[1] TAKAHIRO OTA, M.D.,[1] DAISUKE ITOH, M.D., PH.D.,[2] KENJI INO, R.T.,[2] HIROSHI IGAKI, M.D., PH.D.,[2] SHIGEKI AOKI, M.D., PH.D.,[2] YOSHITAKA MASUTANI, PH.D.,[2] MASAHIRO SHIN, M.D., PH.D.,[1] AND NOBUHITO SAITO, M.D., PH.D.[1]

Departments of [1]Neurosurgery and [2]Radiology, The University of Tokyo Hospital, Tokyo, Japan

Object. To prevent speech disturbances after Gamma Knife surgery (GKS), the authors integrated arcuate fasciculus (AF) tractography based on diffusion tensor (DT) MR imaging into treatment planning for GKS.

Methods. Arcuate fasciculus tractography was retrospectively integrated into planning that had been previously performed by neurosurgeons and radiation oncologists. This technique was retrospectively applied to 12 patients with arteriovenous malformations adjacent to the AF. Diffusion tensor images were acquired before the frame was affixed to the patient's head and DT tractography images of the AF were created using the authors' original software. The data from DT tractography and stereotactic 3D imaging studies obtained after frame fixation were transported to a treatment planning workstation for GKS and coregistered so that the delivered doses and incidence of posttreatment aphasia could be assessed.

Results. The AF could not be depicted in 2 patients who initially presented with motor aphasia caused by hemorrhaging from arteriovenous malformations. During the median follow-up period of 29 months after GKS, aphasia developed in 2 patients: 30 Gy delivered to the frontal portion of the AF caused conduction aphasia in 1 patient, and 9.6 Gy to the temporal portion led to motor aphasia in the other. Speech dysfunction was not observed after a maximum radiation dose of 10.0–16.8 Gy was delivered to the frontal fibers in 4 patients, and 3.6–5.2 Gy to the temporal fibers in 3.

Conclusions. The authors found that administration of a 10-Gy radiation dose during GKS was tolerated in the frontal but not the temporal fibers of the AF. The authors recommend confirmation of the dose by integration of AF tractography with GKS, especially in lesions located near the temporal language fibers.
(DOI: 10.3171/2008.4.17521)

KEY WORDS • **arcuate fasciculus** • **diffusion tensor imaging** • **Gamma Knife surgery** • **treatment planning**

STEREOTACTIC radiosurgery is recognized as an extremely effective treatment modality for vascular, neoplastic, or functional disorders of the brain.[10,16–18] However, radiation-induced neuropathy occurs in 5–20% of patients and can occasionally be disabling, particularly after treatment of lesions in critical locations.[1,5,16,23,25] Although the majority of such complications are due to parenchymal brain injury,[5] there has been no definitive method to prevent it. To help minimize such risks, we developed a novel technique of integrating tractography[19] based on DT MR imaging into treatment planning for GKS. By integrating tractography of the pyramidal tract[13,14] and optic radiation,[15] we have introduced an effective tool for analyzing the effect of GKS on motor and visual function. We hope that this technique will become applicable in the planning of GKS treatment. To our knowledge, there are no other reports of the application of this technique.

The AF connects the frontal and temporal language cortices and a clinically important white matter fiber tract that is only visible with the use of DT tractography.[3,4,7,27] Speech disturbances were observed in 2% of patients after radiosurgery;[12,24] thus the preservation of speech function is a consideration. The tolerated dose of radiation to the AF is unknown, and no definitive method of reducing the risk of these complications has heretofore been available. In the present study we report on our results with the integration of AF tractography into treatment planning for GKS.

Methods

Arcuate fasciculus tractography was retrospectively integrated into planning that had been previously per-

Abbreviations used in this paper: AF = arcuate fasciculus; AVM = arteriovenous malformation; DICOM = Digital Imaging and Communications in Medicine; DT = diffusion tensor; GKS = Gamma Knife surgery.

formed by neurosurgeons and radiation oncologists for GKS in 12 right-handed patients who had been treated for cerebral AVMs located adjacent to the left AF (Table 1). Patients who suffered aphasia after GKS were intentionally selected to enhance the reliability of the dose-response relationship analysis. Written informed consent was obtained from all the patients. All MR imaging studies were performed with a 1.5-T whole-body MR imaging unit with echo planar capabilities and a standard whole-head transmitter–receiver coil (Signa Echospeed, General Electric).

Diffusion Tensor Imaging

Diffusion tensor MR imaging was performed without frame fixation on the day before GKS. In cases in which DT imaging had not been performed, posttreatment images were used instead. We used a single-shot, spin echo-echo planar sequence (TR 6000 msec, TE 78 msec), acquiring 32 interleaved, contiguous 2.5-mm-thick axial images with no cardiac triggering. A data matrix of 128 × 128 pixels over a field of view of 240 × 240 mm was obtained, with 128 echoes acquired per excitation. Diffusion gradients were applied in 13 noncollinear independent axes by using a b value of 0 and 1000 seconds/mm^2. Each echo planar imaging data set required 2 minutes and 48 seconds to obtain and was repeated twice to increase the signal-to-noise ratio. Realignment of the 13 sets of DT images and compensation for the eddy current–induced morphing were performed on the basis of the T2-weighted echo planar imaging set (b = 0) on an equipped workstation connected to the MR imaging unit.

Diffusion Tensor Tractography

Data sets of the realigned DT imaging and the stereotactic imaging studies were transferred to a personal computer equipped with the freely shared software programs Volume-One (Volume-One Developers Group, version 1.72; www.volume-one.org) and dTV (Yoshitaka Masutani, version II; www.ut-radiology.umin.jp/people/masutani/dTV.htm). These programs were used to calculate the DT in each voxel and create DT tractography images. The DT at each pixel of the registered DT imaging data was calculated, and 3D fiber tracking was performed using the freely shared programs. Nine (3 × 3) elements of the symmetrical DT at each voxel were determined by the least-square fit, based on singular value decomposition, and diagonalized to obtain 3 eigenvalues and 3 eigenvectors. An eigenvector associated with the largest eigenvalue was assumed to represent the local fiber orientation. Anisotropy maps were obtained using orientation-independent fractional anisotropy.

Fiber tracking was started from a manually selected start point (a "seed area") from which lines were propagated in both the anterograde and retrograde directions according to an eigenvector at each voxel. The seed area for the AF was selected manually in the deep white matter of the posterior parietal portion of the superior longitudinal fascicle, as described previously.[21,27] A target area was used to limit displayed tracking results to the AF only. The target area was drawn in freehand and encompassed the entire descending portion of the superior longitudinal fascicle in the posterior temporal lobe. Tracking was terminated when a voxel with a fractional anisotropy value of < 0.18 was reached.

After fiber tracking of the AF, only the voxels through which tracts ran were marked and color coded, depending on the fractional anisotropy value of each voxel. The marked voxels of the AF and the T2-weighted echo planar imaging data set were then simply fused and were reformatted using the DICOM format according to the header information on the T2-weighted echo planar imaging studies.

Stereotactic 3D Imaging

On the day of GKS, the patient was immobilized in a Leksell stereotactic coordinate frame and for stereotactic 3D anatomical MR imaging. The MR imaging study consisted of 128 sequential, 1.5-mm-thick axial slices with a resolution of 256 × 256 pixels over a field of view of 240 mm with 3D spoiled-gradient recalled-acquisition in the steady-state sequence. Stereotactic angiography was also performed separately.

Image Integration and Treatment Planning

The T2-weighted echo planar imaging data with tract information, stereotactic imaging data, and the data from stereotactic angiography were transferred via fast ethernet into a treatment planning software, GammaPlan (Elekta Instruments). The T2-weighted echo planar imaging data with tract information and stereotactic imaging data were automatically coregistered by Multiview (Elekta Instruments), a supplementary software to GammaPlan for Gamma Knife 4C. The AF images were black-and-white in the DICOM format and were displayed in orange with GammaPlan to facilitate clear identification. Arcuate fasciculus tractography was thus retrospectively integrated into planning that had been previously performed by neurosurgeons and radiation oncologists. The prescribed dose to the AVM margin had been designed to be ≥ 20 Gy by using 40–50% isodose lines.

Speech function was assessed in all patients before treatment and during the serial clinical follow-up examinations at 6-month intervals after GKS. Any patient who reported a change in speech function underwent a detailed speech function examination. The classification of aphasia was made based on standard diagnostic approaches.[2,8,11] The relationship between the maximum dose delivered to the AF and speech dysfunction was retrospectively reviewed. To analyze the influence of low-dose volumes, we also calculated the volume of AF that received ≥ 8 Gy.

Results

Because of DT imaging characteristics, visualizing the AF was generally more difficult than visualizing the pyramidal tract, and the volume of the AF tended to be smaller than that of the pyramidal tract. In 2 patients, data from DT MR imaging studies obtained after GKS were substituted because DT imaging had not been performed prior to GKS. When the depicted AF was divided length-

TABLE 1: Summary of clinical data in 12 patients who underwent integration of AF tractography into GKS*

Age (yrs), Sex	Location	Presentation	Target Vol (cm^3)	Margin Dose (Gy)	Max Dose to AF (Gy)	8-Gy Vol (mm^3)	FU (mos)	Speech Disturbance
frontal region								
48, M	left parietal	hemorrhage	12.9	20	30.0	613	31	1 mo post-GKS, transient
59, M	left insula	hemorrhage	1.1	20	16.8	58.7	52	—
41, F	left frontal	epilepsy	18.9	17	10.9	125	23	—
27, F	left centrum semiovale	intercranial hypertension	3.5	20	10.8	81.1	27	—
27, F	left frontal	ischemia	11.3	20	10.0	70.9	17	—
53, M	left frontal	incidental	2.5	20	0.8	0	34	—
22, F	left putamen	hemorrhage	0.4	20	NA	NA	23	present before treatment
21, F	left frontal	hemorrhage	2.7	20	NA	NA	17	present before treatment
temporal region								
45, M	left hippocampus	headache	10.3	20	9.6	12.2	34	10 mos post-GKS, transient
47, F	left temporal	hemorrhage	7.3	20	5.2	0	50	—
37, M	left temporal	headache	3.0	20	4.7	0	23	—
49, F	left temporal	headache	2.7	20	3.6	0	42	—

* FU = follow-up; NA = not assessed; 8-Gy Vol = volume of the AF that received ≥ 8 Gy.

wise at its midpoint, the fiber location primarily affected by the lesion was the frontal white matter in 8 patients and the temporal in 4. The AF could not be visualized in 2 patients who presented with motor aphasia caused by hemorrhaging from AVMs located in the frontal lobe and the putamen, respectively. Patients were followed up for 17–52 months (median 29 months). Two patients suffered a hemorrhage during the latency period until obliteration, but the hemorrhage did not affect speech functioning in either patient. Serial T2-weighted images showed transient or permanent perilesional edema in 3 of 12 patients. One of these patients remained asymptomatic throughout the clinical course of 28 months, but the other 2 developed speech dysfunction after GKS; these patients are described below.

Speech Dysfunction After GKS

A 48-year-old man who underwent GKS for a ruptured parietal AVM developed a speech disturbance 1 month postoperatively. He had received a 20-Gy radiation dose to the margin. A detailed examination revealed literal paraphasia, moderately impaired verbal fluency, poor repetition, and normal comprehension. His symptoms were considered to indicate conduction aphasia.[2,8,11] Neuroimaging studies demonstrated a mild adverse radiation effect in the parietal paraventricular territory surrounding the AVM nidus (Fig. 1). The conduction aphasia gradually improved, and he recovered fully over a clinical course of 4 months. According to our retrospective analysis, the frontal portion of the AF had been irradiated with 30.0 Gy at a maximum, and the dose to the language cortex was 2.9 Gy in the Broca area and 0.6 Gy in the Wernicke area.

The other patient in whom speech dysfunction arose was a 45-year-old man with an unruptured temporal AVM. Wada testing performed before GKS confirmed the left side to be his dominant hemisphere. Ten months after a dose of 20 Gy had been administered to the AVM margin, this patient began to experience speech and handwriting difficulties. Naming was poor but comprehension was intact and his symptoms were considered Broca aphasia.[2,8,11] Neuroimaging studies demonstrated a severe adverse radiation effect in the wide subcortical area around the left temporal AVM (Fig. 2). The aphasia gradually improved, and the patient fully recovered over a clinical course of 9 months. Our retrospective analysis indicated that the maximum dose to the temporal portion of the AF was 9.6 Gy. The dose to the language cortex was 2.7 Gy in the Broca area, and 3.6 Gy in the Wernicke area. In both patients with postoperative speech dysfunction, 20 Gy was delivered to a volume > 10 cm^3.

The remaining 8 patients did not show speech disturbances during the clinical course (Fig. 3). The maximum dose to the AF was 10.0–16.8 Gy to the frontal fiber in 4 patients and 3.6–5.2 Gy to the temporal fibers in 3. A high dose of ≥ 20 Gy was delivered to an 11.2 cm^3 volume in a patient who received 17 Gy to 18.9 cm^3. Of 8 patients who did not experience dysphasia, 20 Gy was delivered to a volume of > 10 cm^3 in 2. As the volume of the AF that received ≥ 8 Gy increased, the maximum dose to the AF tended to increase. No patient suffered speech disturbances after receiving a relatively low dose of radiation to a large volume (Table 1). Logistic regression analysis was performed to analyze the relationship of the maximum dose to the AF and speech dysfunction, but no significant correlation was found.

Discussion

In our experience with this limited cohort, aphasia was observed after irradiation of 9.6 Gy to the temporal fibers and 30 Gy to the frontal fibers of the AF, but

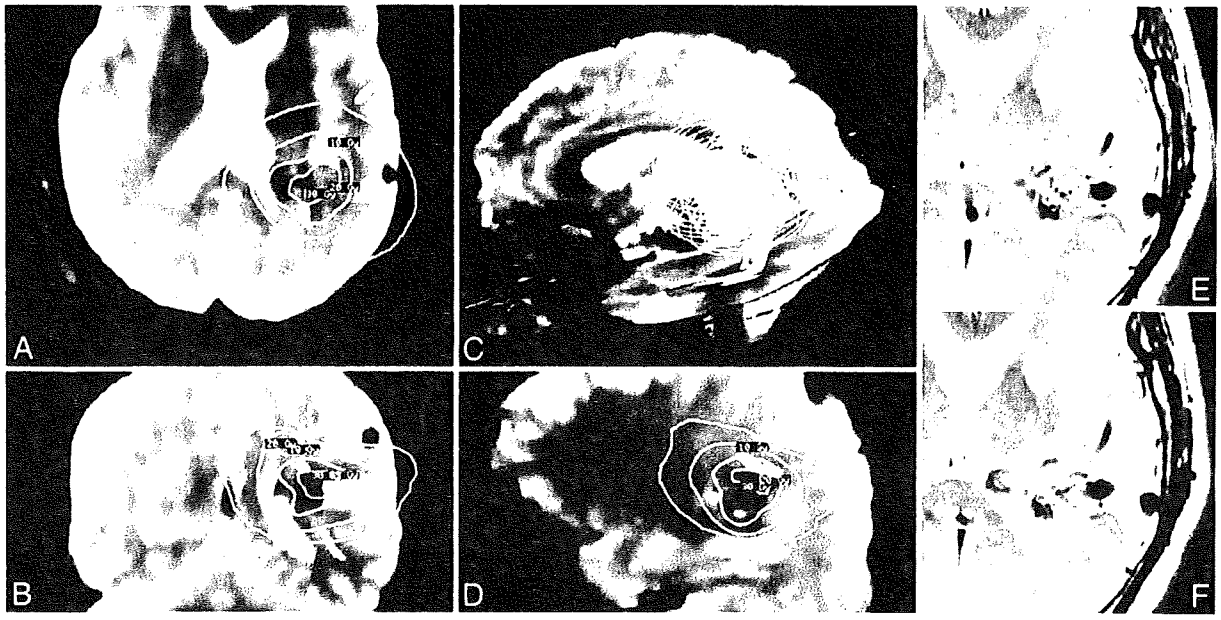

FIG. 1. Axial (A), coronal (B), 3D reconstruction image (C), and sagittal (D) radiosurgical dosimetry studies on T2-weighted MR images showing the results of integrating the AF tractography (with the AF shown in *orange*) in a 48-year-old man who developed conduction aphasia 1 month after GKS. The maximum dose to the AF was 30.0 Gy. The spatial relationship between the dose distribution and the AF is clearly demonstrated in the 3D MR reconstruction. The *yellow object* in C represents the volume that received 20 Gy. The *green* and *light blue mesh* correspond to the volumes that received 10 and 5 Gy, respectively. Comparison of image obtained before GKS (E) with that obtained 1 month postoperatively (F) demonstrates a mild adverse radiation effect.

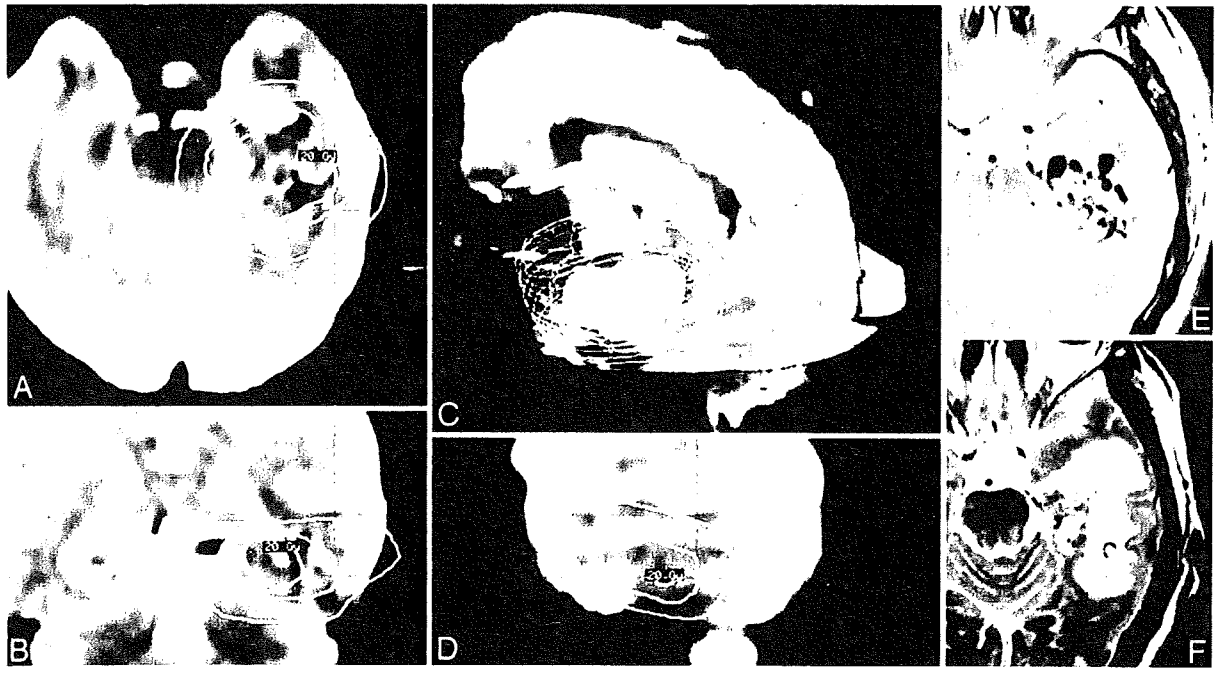

FIG. 2. Axial (A), coronal (B), 3D reconstruction image (C), and sagittal (D) radiosurgical dosimetry studies on T2-weighted MR images showing the results of AF tractography integration with GKS planning in a 45-year-old man who developed Broca aphasia 10 months postoperatively. The maximum dose to the AF was 9.6 Gy. In the 3D reconstruction (C), the *yellow object* represents the volume that received 20 Gy. The *green* and *light blue mesh* correspond to the volumes that received 10 and 5 Gy, respectively. Comparison of the image obtained before GKS (E) with that obtained 10 months postoperatively (F) demonstrates a severe adverse radiation effect.

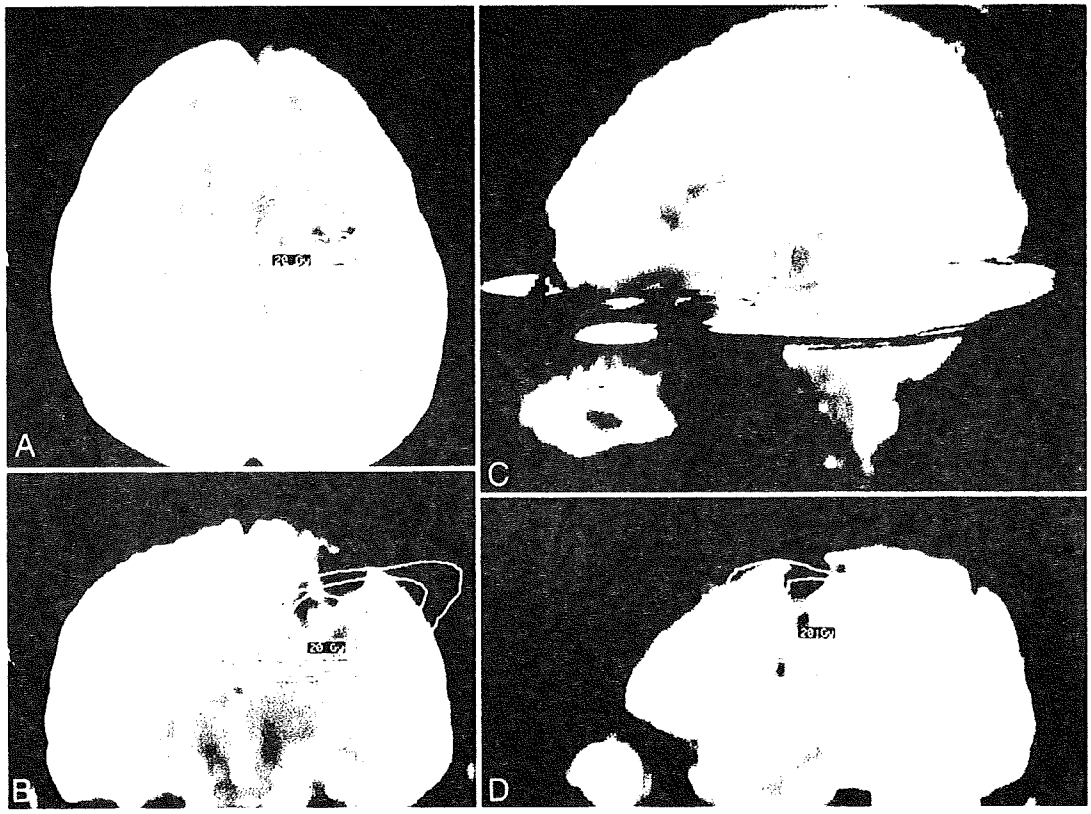

FIG. 3. A–D: Radiosurgical dosimetry studies on T2-weighted MR images showing the results of AF tractography integration in a 27-year-old woman with a left frontal AVM who received a maximum dose of 10.0 Gy to the AF *(orange)*. The patient experienced no complications during 17 months of follow-up after GKS. In the 3D reconstruction (C), the *yellow object* represents the volume that received 20 Gy. The *green mesh* and the *light blue mesh* correspond to the volumes that received 10 and 5 Gy, respectively.

not after 10–16.8 Gy was delivered to the frontal fibers. Thus, it seems that the threshold of AF radiation tolerance differs between the frontal and temporal fibers. That is, tolerance to GKS was suggested to be lower in the temporal fibers than in the frontal fibers. According to reports on the cranial nerves, tolerance to radiosurgery is lower in the sensory nerves than the motor nerves,[9,20] and the results of this study were consistent with these findings when the sensory nerves are regarded as the input fibers and the motor nerves as the output fibers. Additionally, it is interesting to note that the dose threshold of the frontal and temporal portions of the AF was almost similar to that of the optic radiation[15] (input fibers) and the pyramidal tract[13,14] (output fibers), respectively. The dose-complication relationship was not correlated to the logistic regression curves, and the dose threshold was not calculated for the AF. This might be because the number of patients suffering from aphasia was small. Although definitive conclusions on radiation tolerance cannot be drawn from our limited experience, no other institutes have reported a similar effort and this technique is possible only at our institution. Our study results will undoubtedly provide fundamental data that can be used in future studies concerning the tolerance of the frontotemporal language fibers to radiation. The follow-up in our patients is also relatively limited, and the long-term consequences of radiation to this white matter tract remain unknown. More detailed information on radiation tolerance must be clarified by further advances in neuroimaging techniques and the accumulation of data in more patients with a longer follow-up.

Because the dose to the language cortices was sufficiently low in 2 patients who suffered speech dysfunction, aphasia could be attributable to a direct radiation injury to the AF. As 1 patient developed aphasia 1 month after GKS for radiation injury, other kinds of complications such as seizures could be part of the differential diagnosis. However, adverse radiation effects were confirmed on neuroimaging studies and the 4-month recovery period was compatible with radiation injury, although a definitive diagnosis could not be rendered without obtaining a surgical specimen. In the 2 patients who suffered aphasia, 20 Gy was applied to a volume of > 10 cm^3. Because a high dose was delivered to a wide area of the AF, the high radiation dose could be related to aphasia. Remarkably, injury to the frontal fibers resulted in conduction aphasia, a typical symptom of damaging the AF, while injury of the temporal fibers did not lead instead to motor aphasia, a condition for which no formal speech function examination is performed. The reasons for this finding remain speculative; the semantic system is composed of more complex connecting and associating fibers than the

simple input or output fibers, such as the optic radiation or the pyramidal tract.[4] An injury to the AF fibers might not necessarily cause language dysfunction because language processing requires the participation of a distributed neural system in the left hemisphere.[4,26]

There exist several limitations in the AF tractography. The AF could not be visualized in 2 patients who presented with aphasia before treatment, which was consistent with findings in a previous report.[3] In general, DT tractography is not suitable for describing bending or crossing fibers such as the AF or the optic radiation.[3,22] Narrowing of the AF in the presence of an AVM has also been examined both qualitatively[3,6] and quantitatively,[22] and the existence of several branching of the AF.[4] Additionally, the extent of depicting the AF depends on language dominance.[21,27] Thus, it is possible that only part of the AF could be visualized. Another issue is whether the depicted tracts represent true language fibers. To solve these problems, AF tractography was validated with intraoperative electrical stimulation during awake surgery at our institute.[7] The addition of functional MR imaging or magnetoencephalography studies conducted before treatment would enhance the reliability of preoperative AF localization and enable appropriate selection of the seed and target points.[7]

By a series of clinical simulation studies including this one, we have integrated tractography studies into GKS dosimetry plots.[13–15] We expect that this technique will be applied in the wide variety of stereotactic radiosurgical procedures including linear accelerator radiosurgery, and we hope that the safety of stereotactic radiosurgery will be improved as a result.

Conclusions

In our experience with a limited cohort, the administration of 10 Gy during GKS was tolerated in the frontal but not in the temporal fibers of the AF. Based on this observation, confirmation of the dose to be delivered by integrating AF tractography into GKS is recommended, especially in lesions located adjacent to the temporal language fibers.

Disclosure

This work was supported in part by Takeda Science Foundation and grants-in-aid for scientific research awarded to Dr. Maruyama from the Ministry of Education, Science, and Culture of Japan (Grant No. 18791013).

References

1. Andrade-Souza YM, Zadeh G, Scora D, Tsao MN, Schwartz ML: Radiosurgery for basal ganglia, internal capsule, and thalamus arteriovenous malformation: clinical outcome. **Neurosurgery 56:**56–64, 2005
2. Benson DF: Aphasia, in Heilman KM, Valenstein E (eds): **Clinical Neuropsychology, ed 3.** New York: Oxford University Press, 1993, pp 17–36
3. Berube J, McLaughlin N, Bourgouin P, Beaudoin G, Bojanowski MW: Diffusion tensor imaging analysis of long association bundles in the presence of an arteriovenous malformation. **J Neurosurg 107:**509–514, 2007
4. Catani M, Jones DK, ffytche DH: Perisylvian language networks of the human brain. **Ann Neurol 57:**8–16, 2005
5. Flickinger JC, Kondziolka D, Lunsford LD, Pollock BE, Yamamoto M, Gorman DA, et al: A multi-institutional analysis of complication outcomes after arteriovenous malformation radiosurgery. **Int J Radiat Oncol Biol Phys 44:**67–74, 1999
6. Itoh D, Aoki S, Maruyama K, Masutani Y, Mori H, Masumoto T, et al: Corticospinal tracts by diffusion tensor tractography in patients with arteriovenous malformations. **J Comput Assist Tomogr 30:**618–623, 2006
7. Kamada K, Todo T, Masutani Y, Aoki S, Ino K, Morita A, et al: Visualization of the frontotemporal language fibers by tractography combined with functional magnetic resonance imaging and magnetoencephalography. **J Neurosurg 106:**90–98, 2007
8. Kertesz A: Aphasia, in Vinken PJ, Bruyn GW, Klawans HL (eds): **Handbook of Clinical Neurology.** Amsterdam: Elsevier Science Publishers, 1985, Vol 45, pp 287–331
9. Leber KA, Bergloff J, Pendl G: Dose-response tolerance of the visual pathways and cranial nerves of the cavernous sinus to stereotactic radiosurgery. **J Neurosurg 88:**43–50, 1998
10. Leksell L: Cerebral radiosurgery. I. Gammathalamotomy in two cases of intractable pain. **Acta Chir Scand 134:**585–595, 1968
11. Lindsay KW, Bone I: Disorder of language—dysphasia, in Lindsay KW, Bone I (eds): **Neurology and Neurosurgery Illustrated.** New York: Churchill Livingstone, 1997, p 120
12. Loeffler JS, Siddon RL, Wen PY, Nedzi LA, Alexander E III: Stereotactic radiosurgery of the brain using a standard linear accelerator: a study of early and late effects. **Radiother Oncol 17:**311–321, 1990
13. Maruyama K, Kamada K, Ota T, Koga T, Itoh D, Ino K, et al: Tolerance of pyramidal tract to gamma knife radiosurgery based on diffusion-tensor tractography. **Int J Radiat Oncol Biol Phys 70:**1330–1335, 2008
14. Maruyama K, Kamada K, Shin M, Itoh D, Aoki S, Masutani Y, et al: Integration of three-dimensional corticospinal tractography into treatment planning for gamma knife surgery. **J Neurosurg 102:**673–677, 2005
15. Maruyama K, Kamada K, Shin M, Itoh D, Masutani Y, Ino K, et al: Optic radiation tractography integrated into simulated treatment planning for Gamma Knife surgery. **J Neurosurg 107:**721–726, 2007
16. Maruyama K, Kawahara N, Shin M, Tago M, Kishimoto J, Kurita H, et al: The risk of hemorrhage after radiosurgery for cerebral arteriovenous malformations. **N Engl J Med 352:**146–153, 2005
17. Maruyama K, Kondziolka D, Niranjan A, Flickinger JC, Lunsford LD: Stereotactic radiosurgery for brainstem arteriovenous malformations: factors affecting outcome. **J Neurosurg 100:**407–413, 2004
18. Maruyama K, Shin M, Kurita H, Kawahara N, Morita A, Kirino T: Proposed treatment strategy for cavernous sinus meningiomas: a prospective study. **Neurosurgery 55:**1068–1075, 2004
19. Masutani Y, Aoki S, Abe O, Hayashi N, Otomo K: MR diffusion tensor imaging: recent advance and new techniques for diffusion tensor visualization. **Eur J Radiol 46:**53–66, 2003
20. Morita A, Coffey RJ, Foote RL, Schiff D, Gorman D: Risk of injury to cranial nerves after gamma knife radiosurgery for skull base meningiomas: experience in 88 patients. **J Neurosurg 90:**42–49, 1999
21. Nucifora PG, Verma R, Melhem ER, Gur RE, Gur RC: Leftward asymmetry in relative fiber density of the arcuate fasciculus. **Neuroreport 16:**791–794, 2005
22. Okada T, Miki Y, Kikuta K, Mikuni N, Urayama S, Fushimi Y, et al: Diffusion tensor fiber tractography for arteriovenous malformations: quantitative analyses to evaluate the corticospinal tract and optic radiation. **AJNR Am J Neuroradiol 28:**1107–1113, 2007

23. Pollock BE, Gorman DA, Brown PD: Radiosurgery for arteriovenous malformations of the basal ganglia, thalamus, and brainstem. **J Neurosurg 100:**210–214, 2004
24. Regis J, Bartolomei F, Kida Y, Kobayashi T, Vladyka V, Liscak R, et al: Radiosurgery for epilepsy associated with cavernous malformation: retrospective study in 49 patients. **Neurosurgery 47:**1091–1097, 2000
25. Sasaki T, Kurita H, Saito I, Kawamoto S, Nemoto S, Terahara A, et al: Arteriovenous malformations in the basal ganglia and thalamus: management and results in 101 cases. **J Neurosurg 88:**285–292, 1998
26. Shaywitz BA, Shaywitz SF, Pugh KR, Constable RT, Skudlarski P, Fulbright RK, et al: Sex differences in the functional organization of the brain for language. **Nature 373:**607–609, 1995
27. Vernooij MW, Smits M, Wielopolski PA, Houston GC, Krestin GP, van der Lugt A: Fiber density asymmetry of the arcuate fasciculus in relation to functional hemispheric language lateralization in both right- and left-handed healthy subjects: a combined fMRI and DTI study. **Neuroimage 35:**1064–1076, 2007

Manuscript submitted February 11, 2008.
Accepted April 14, 2008.
Please include this information when citing this paper: published online November 21, 2008; DOI: 10.3171/2008.4.17521.

Address correspondence to: Keisuke Maruyama, M.D., Ph.D., Department of Neurosurgery, The University of Tokyo Hospital, 7-3-1 Hongo, Bunkyo-ku, Tokyo 113-8655, Japan. email: kskmaru-tky@umin.ac.jp.

Dose profile measurement using an imaging plate: Evaluation of filters using Monte Carlo simulation of 4 MV x-rays

Masatoshi Hashimoto,[1,2,a)] Tetsuya Tomita,[3] Koichi Sawada,[3] Toshioh Fujibuchi,[4] Teiji Nishio,[5] and Keiichi Nakagawa[1]

[1]*Division of Radiology and Biomedical Engineering, Graduate School of Medicine, The University of Tokyo, Bunkyo-ku, Tokyo 113-8655, Japan*

[2]*Department of Therapeutic Radiology, Medical Plaza Edogawa, Edogawa-ku, Tokyo 133-0052, Japan*

[3]*Department of Radiology, Chiba University Hospital, Cyuo-ku, Chiba 260-8677, Japan*

[4]*Department of Radiological Sciences, School of Health Science, Ibaraki Prefectural University, Inashiki-gun, Ibaraki 300-0394, Japan and Graduate School of Comprehensive Human Sciences, University of Tsukuba, Tsukuba-shi, Ibaraki 305-8575, Japan*

[5]*Particle Therapy Division, Research Center for Innovation Oncology, National Cancer Center Hospital East, Kashiwa-shi, Chiba 277-8577, Japan*

(Received 1 December 2008; accepted 1 March 2009; published online 7 April 2009)

Computed radiography (CR) is gradually replacing film. The application of CR for two-dimensional profiles and off-axis ratio (OAR) measurement using an imaging plate (IP) in a CR system is currently under discussion. However, a well known problem for IPs in dosimetry is that they use high atomic number (Z) materials, such as Ba, which have an energy dependency in a photon interaction. Although there are some reports that it is possible to compensate for the energy dependency with metal filters, the appropriate thicknesses of these filters and where they should be located have not been investigated. The purpose of this study is to find the most suitable filter for use with an IP as a dosimetric tool. Monte Carlo simulation (Geant4 8.1) was used to determine the filter to minimize the measurement error in OAR measurements of 4 MV x-rays. In this simulation, the material and thickness of the filter and distance between the IP and the filter were varied to determine most suitable filter conditions that gave the best fit to the MC calculated OAR in water. With regard to changing the filter material, we found that using higher Z and higher density material increased the effectiveness of the filter. Also, increasing the distance between the filter and the IP reduced the effectiveness, whereas increasing the thickness of the filter increased the effectiveness. The result of this study showed that the most appropriate filter conditions consistent with the calculated OAR in water were the ones with the IP sandwiched between two 2 mm thick lead filters at a distance of 5 mm from the IP or the IP sandwiched directly between two 1 mm lead filters. Using these filters, we measured the OAR at 10 cm depth with 100 cm source-to-surface distance and surface 10×10 cm^2 field size. The results of this measurement represented that it is possible to achieve measurements with less than within 2.0% and 2.0% in the field and with less than 1.1% and 0.6% out of the field by using 2 and 1 mm lead filters, respectively. © *2009 American Institute of Physics.* [DOI: 10.1063/1.3103572]

I. INTRODUCTION

For radiation therapy, it is important to measure the dose distribution in materials in order to put together a treatment plan that will give an accurate dose distribution and ensure that the dose to normal tissue is minimized. The usual way to measure this is to use an ion chamber in water as a gold standard. However, because this is a sort of point measurement, it is time-consuming to measure the off-axis ratio (OAR) in two or three dimensions. Furthermore, the resolution of scans is limited due to chamber size.

To measure the dose distribution with high spatial resolution the use of film is an easier solution.[1–4] However, the film needs to be developed, and requires that the film processor be maintained. With GafChromic film,[5–7] it may be much easier and more useful because of no need to be chemical processing; however, all facilities cannot afford to purchase the film digitizer and use such expensive films constantly as a quality assurance tool. On the other hand, computed radiography (CR) system,[8] which has been originally used for diagnostic purpose, has been more widely used than GafChromic film. Additionally, it is being discussed that CR becomes more prevalent in radiotherapy. The use of the film processor is decreasing.

A new dosimetric method using an imaging plate[9,10] (IP) in a CR system has recently been considered as a replacement for film,[11–13] with the advantage that this method does not need a film processor. However, IPs include high atomic number (high Z) materials such as barium, for which there is, in general, an energy dependency problem, which can produce an error in the measurements. It is reported that similar errors occur even in film measurements, but it is possible to

a)Electronic mail: m_hashimoto@movie.ocn.ne.jp.

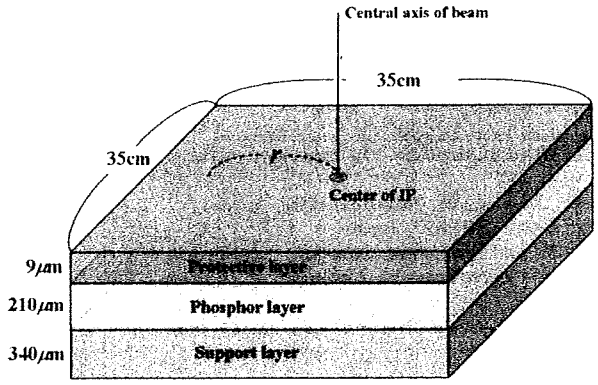

FIG. 1. Structure of the IP used in the MC simulation composed of three layers, a protective layer, a phosphor layer, and a support layer, respectively. r is the distance from the center of IP. The center of IP is corresponding to the central axis of x-ray.

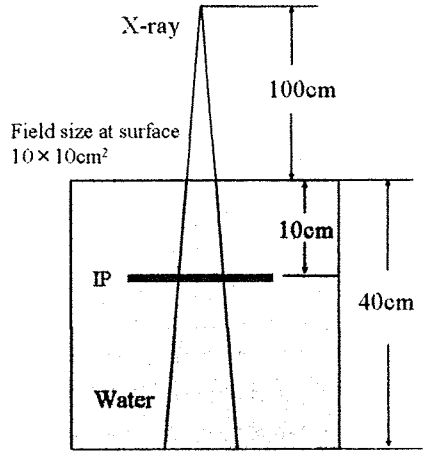

FIG. 2. Materials setting. A $40\times40\times40$ cm^3 water tank phantom was used in the simulation. The SSD was 100 cm and the field size 10×10 cm^2. The middle of water phantom was irradiated with a 4 MV photon beam. The incidence of photons was uniformly carried out in the exposure field. The IP was place at a depth of 10 cm from the surface of water.

compensate these errors with metal filters.[14–16] There has been a report asserting that filters can be used to compensate the errors for IP measurements also.[11] Nevertheless a detailed discussion regarding the kind of materials to use or where the filters should be placed, etc. has not taken place. The purpose of this study is to use Monte Carlo (MC) simulation to determine the most appropriate filter for IP measurements. In this investigation, we attempt to find the most appropriate material, thickness, and location of the filter for IP dosimetry in order to minimize the dosimetric error in OAR measurements with a 4 MV photon beam.

II. MATERIALS AND METHODS

A. MC simulation parameter settings and evaluation

For the MC simulations, we used GEANT4 (version 8.1 patch-01). GEANT4 is a calculation code widely used for high energy physics, nuclear physics, space physics, and medical physics, etc. The photon and electron interactions in the material are simulated down to 250 eV.[17] The GEANT4 physics models selected for this study were the low-energy electromagnetic process, and the number of history was 2×10^8 photons. GEANT4 utilizes a stopping range instead of energy to control the tracking and production of secondaries. In GEANT4, all particles are tracked to a zero range except for secondaries with a range shorter than the production cutoff range set by the user. In this study, the production cutoff range was set to 0.01 mm.

The spectrum used in this study was a 4 MV photon spectrum calculated from Schiff's formula.[18] There have been reports that this formula has been extended for medical linear accelerator.[19–21] In this study, we calculated the spectrum using Schiff's formula, where we attached 10 mm thick copper attenuations by every 50 keV as the target and the material under the target.

The IP used in the MC simulation is a ST-VN (FUJIFILM Corp., Minato-ku, Tokyo). As shown in Fig. 1 the size of the IP is $35\times35\times0.0559$ cm^3 and it is composed of three layers, a protective, phosphor, and support layer and protective and support layers are made of Polyethylene terephthalate (PET), and the phosphor layer is BaFBrI. The composition of PET is C:H:O=10:8:4 and the density is 1.38 g/cm^3. BaFBrI consists of 56.45% Ba, 7.81% F, 27.92% B, 7.82% I, and the density was set to 5.50 g/cm^3. To verify the calculation conditions, we compared measurements and simulation.

1. Measurement

The linear accelerator used was Clinac2100C (Varian Medical Systems Inc., Palo Alto, CA) and we used only 4 MV photons with a 10×10 cm^2 field and a 100 cm source-to-surface distance (SSD). For percentage depth dose (PDD) measurements in water, we used a PTW Freiburg N31005 ionization chamber in a three-dimensional (3D) water phantom (Dynascan, Computerized Medical Systems Inc., St. Louis, MO). We measured the PDD on the central beam axis and the OAR at a depth of 10 cm. For the OAR measurement with the IP, a 40×40 cm^2 water equivalent solid phantom (Solid Water Phantom, Gammex Inc., Middleton, WI) was used instead of the 3D water phantom. The IP (ST-VN, 35×35 cm^2, Fujifilm Corp., Minato-ku, Tokyo) was placed perpendicular to the beam axis at a depth of 10 cm in the stack of 40 cm solid phantom. The IP was exposed to a dose of 12.5 mGy, and was then read out using a FCR5000 (Fujifilm Medical Co. Ltd., Minato-ku, Tokyo) and converted to DICOM format where the S value, which gives the sensitivity of the FCR during read out, was set to 2, and the L value, which gives the latitude, was set to 4. The other parameter settings were S-Shift:1, C-Shift:1, GA:A, GC:1.2, GS:0.00, RN:3, RT: F, RE:0.0, and DRC: off. These values were all fixed. The OAR data were obtained from a line profile on the acquired two-dimensional IP dose profiles. To determine the dose deposited on the IP we made the dose conversion table for the pixel value on the IP. First we measured at the central axis with an ion chamber from 2.5 to 15 mGy under the same condition, and next we read out the